LASER & PHOTONICS REVIEWS

www.lpr-journal.org

Nonlinear Moiré Superlattice for Super-Resolution Nondestructive Detection of Nonlinear Photonic Crystals

*Haigang Liu and Xianfeng Chen**

The moiré effect is a universal phenomenon originating from the interference of waves, and it is widely applied in metrology as well as superconductor phenomena in graphene. The present study demonstrates a nonlinear moiré effect originating from the moiré superlattices of two nonlinear photonic crystals (NPCs). It is experimentally shown that these nonlinear moiré superlattices facilitate the nondestructive detection of nonlinear photonic crystals. Two identical periodically poled lithium niobates (PPLNs) are used to observe the nonlinear moiré effect originating from the nonlinear moiré superlattices. This is followed by a demonstration of the detection capability of the nonlinear optical method for dissimilar PPLNs and calculation of the period detection range. The theoretically and experimentally obtained periods of the target PPLN are consistent, and the resolution of the nonlinear moiré effect surpasses to that of presently used optical systems. Furthermore, the detection range of the nonlinear moiré effect enables the sub-micrometer- and nanometer-scale detection of the nonlinear photonic crystal structure using only an optical microscope. The present study conceptually extends the conventional moiré lattice to nonlinear optics, and it can also be extended to other fields where nonlinear effects cannot be avoided, such as polaritons and Bose–Einstein condensates.

1. Introduction

The moiré effect is a universal phenomenon that was observed back in the 18th century. It is caused by the interference of waves and has been widely observed for optical waves,[1] surface plasmon polaritons,[2] X-rays,[3] and even matter waves.[4] The moiré effect has been extensively used in precision metrology owing to its high sensitivity to object displacement.[5] Recently, it has attracted significant attention owing to the discovery of the outstanding physical phenomena in moiré lattices. These phenomena include unconventional superconductivity and quantum Hall effect in graphene moiré superlattices,[6,7] localization and delocalization of light in photonic moiré lattices,[8] moiré excitons in van der Waals heterostructures,[9] and intrinsic quantized anomalous Hall effect in moiré heterostructures.[10]

Nonlinear photonic crystals (NPCs) are special materials in which the second-order susceptibility ($\chi^{(2)}$) is spatially modulated, while the linear susceptibility remains constant.[11–13] They were initially reported by Bloembergen as a means to increase the conversion efficiency in nonlinear frequency conversion process.[14] Presently, NPCs play an important role in nonlinear optics because their ability to get the high-brightness coherent radiation extending from infrared to ultraviolet light by designing the period structures.[15,16] Broadband nonlinear harmonic waves can also be achieved using specially designed NPCs.[17,18] Moreover, random quasiphase matching can be achieved in bulk polycrystalline isotropic nonlinear materials that are composed of randomly distributed domains.[19] In addition to their ability to get coherent or incoherent light source, these special crystals exhibit certain fundamental phenomena of nonlinear optics, such as nonlinear Raman–Nath diffraction,[20,21] nonlinear Cherenkov radiation,[22,23] nonlinear Huygens–Fresnel principle,[24] nonlinear Talbot effect,[25] and nonlinear volume holography.[26] Recently, the manipulation of nonlinear harmonic waves has also been achieved using the structural properties of NPCs such as nonlinear vortex and Airy beam generation.[27,28] NPCs exhibit interesting phenomena in not only classical optics but also quantum optics. These crystals can be used to produce high-brightness quantum light sources and manipulate quantum states.[29–31] Furthermore, the future development of integrated photonics increases the scope of applications for specially designed NPCs.[32–34]

The importance of the detection methods for NPCs has increased with the extensive application of these crystals in various fields. In previous studies, the structure of NPCs was detected using a common optical microscope after etching with hydrofluoric acid, which is a common destructive detection method.[24,26,35,36]

Dr. H. Liu, Prof. X. Chen
State Key Laboratory of Advanced Optical Communication Systems and Networks
School of Physics and Astronomy
Shanghai Jiao Tong University
Shanghai 200240, China
E-mail: xfchen@sjtu.edu.cn
Prof. X. Chen
Shanghai Research Center for Quantum Sciences
Shanghai 201315, China
Prof. X. Chen
Jinan Institute of Quantum Technology
Jinan 250101, China
Prof. X. Chen
Collaborative Innovation Center of Light Manipulations and Applications
Shandong Normal University
Jinan 250358, China

DOI: 10.1002/lpor.202000596

To avoid destruction of the original structures, a nondestructive method was proposed for the detection of NPCs using nonlinear Cherenkov radiation.[37] The nonlinear Talbot effect can be applied as a lens-less imaging method for the nondestructive detection of NPCs, thereby significantly simplifying the experimental setup.[25] An nearly diffraction-free effect of the domain wall is proposed in such a nonlinear image process, which provides a simple way to realize high-resolution imaging of ferroelectric domains.[38] However, these optical methods for the detection of NPCs are limited by the resolution of the optical system used. The advent of nanophotonics in recent years has induced a continuous decrease in the required sizes of NPCs.[34,39] Nonoptical methods, such as piezoresponse force microscopy[40] and Raman confocal microscopy,[41,42] are used for the detection of NPCs at the micro- or nanoscale. However, these methods are expensive and require complex operation of the samples. Therefore, it is crucial to develop a new optical method with a resolution superior to that of the existing optical methods to facilitate the nondestructive detection of NPCs.

In the present study, we reported the application of a moiré superlattice in second-order nonlinear optical parametric processes and demonstrated the super-resolution nondestructive detection of NPCs using the nonlinear moiré effect of the nonlinear moiré superlattice. When only one NPC was placed in our homemade imaging system, the structure was not clearly detected using a second-harmonic (SH) signal. However, the structure information was reconstructed using the nonlinear moiré effect. Thereafter, we calculated the detection range of this method using an optical microscope with a resolution of 1 μm. The results revealed the successful detection of micro- and nanoscale structures of NPCs.

2. Results

2.1. Nonlinear Moiré Effect Observed in the Nonlinear Moiré Superlattice

The schematic of the formation of the nonlinear moiré effect in the nonlinear moiré superlattice is shown in **Figure 1**. The second-order nonlinearity coefficient for a periodically modulated nonlinear structure can be represented as

$$\chi^{(2)} = d_{ij}\,\mathrm{sign}\left[\cos\left(2\pi f x\right)\right] \tag{1}$$

where d_{ij} is an element of the quadratic susceptibility $\chi^{(2)}$ tensor. $f = 1/\Lambda$ is the spatial frequency of the nonlinear structure, and Λ represents its period. x is the x-coordinate of the NPCs. Considering a paraxial and undepleted approximation of the fundamental frequency (FF) wave, the coupled wave equation can be written as

$$\frac{\mathrm{d}E(2\omega)}{\mathrm{d}z} = \frac{2\mathrm{i}\omega^2}{c^2 k_2}\chi^{(2)}E^2(\omega)\,\mathrm{e}^{\mathrm{i}\Delta k z} \tag{2}$$

where $E(\omega)$, $E(2\omega)$, ω, and c denote the incident FF light, generated SH wave, angular frequency, and light speed in vacuum. Furthermore, $\Delta k = 2k_1 - k_2$ represents the phase mismatch between the FF wavevector (k_1) and the SH wavevector (k_2). The generated SH is directly proportional to the $\chi^{(2)}$ structure when

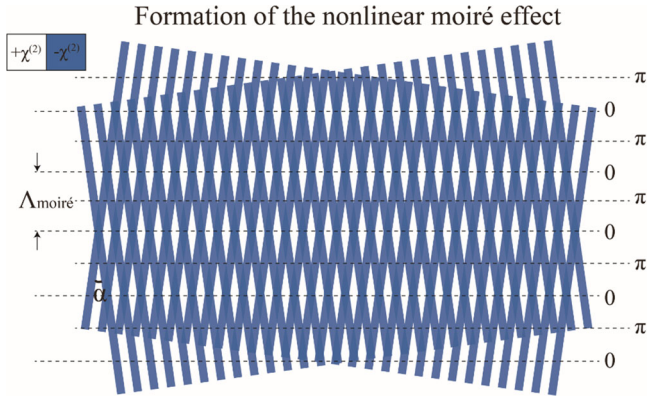

Figure 1. Schematic of the formation of the nonlinear moiré effect in the nonlinear moiré superlattice. Two periodically poled NPCs ($\chi^{(2)}$ structure) are superimposed with an angle α. The 0-phase line represents the location of same ferroelectric domains in the two NPCs that constructively interfere for the generated SH. The π-phase line represents the location of opposite ferroelectric domains in the two NPCs that destructively interfere for the generated SH. $\Lambda_{\mathrm{moiré}}$ is the period of nonlinear moiré effect.

the FF light is incident along the z-axis of the crystal. This results in a phase change of the adjacent domain areas. Considering only the positive ferroelectric domain area (0-phase part of the generated SH) of the periodically modulated nonlinear crystal, the SH transmittance function in the imaging plane exhibits periodic behavior and can be written as

$$T(2\omega) \propto 0.5 \cdot \left\{1 + \mathrm{sign}\left[\cos\left(2\pi f x\right)\right]\right\} \tag{3}$$

When two NPCs with different periods are tightly superimposed, the total SH transmittance function can be written as

$$\begin{aligned} T_{\mathrm{total}}(2\omega) \propto T_1(2\omega)\,T_2(2\omega) \propto 0.25 \cdot \Big\{1 &+ \mathrm{sign}\left[\cos\left(2\pi f_1 x\right)\right] \\ &+ \mathrm{sign}\left[\cos\left(2\pi f_2 x\right)\right] + 0.5 \cdot \mathrm{sign}\left[\cos\left[2\pi\left(f_1 + f_2\right)x\right]\right] \\ &+ 0.5 \cdot \mathrm{sign}\left[\cos\left[2\pi\left(f_1 - f_2\right)x\right]\right]\Big\} \end{aligned} \tag{4}$$

The first term represents uniform transmittance. The second and third terms represent the structural properties of individual nonlinear gratings. The fourth and fifth terms are, respectively, the sum and different frequency terms of the nonlinear spatial structure. The different frequency term is responsible for origination of the nonlinear moiré effect. Moreover, this term presents the required information owing to the relatively low spatial frequency of the SH wave, which is easy to observe. Generally, when two nonlinear gratings are superimposed with an angle α, the period of the corresponding nonlinear moiré pattern can be represented as

$$\Lambda_{\mathrm{moiré}} = \left(\Lambda_1\Lambda_2\right) / \left(\sqrt{\Lambda_1^2 + \Lambda_2^2 - 2\Lambda_1\Lambda_2\cos\alpha}\right) \tag{5}$$

where Λ_1 and Λ_2 are the periods of the two nonlinear gratings. It is important to note that only the nonlinear moiré pattern with a positive ferroelectric domain area (0-phase part) is analyzed in the equations above, as denoted by the 0-phase line in Figure 1. This is because the results are identical to those obtained via

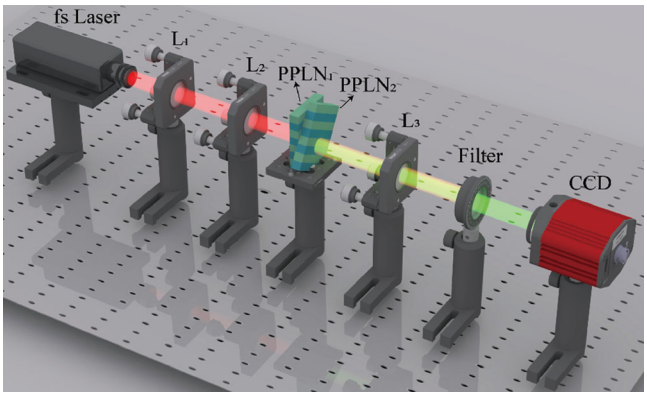

Figure 2. Schematic of the experimental setup. L_{1-3}: lens; f_1, f_2, and f_3 are 200, 100, and 50 mm, respectively; L_3 and CCD camera constitute an imaging system of unit magnification. The two periodically poled lithium niobate (PPLN) samples exhibit the nonlinear moiré effect, without loss of generality.

analysis of the nonlinear moiré pattern with a negative ferroelectric domain area. It is usually difficult to detect phase information using a charge-coupled device (CCD) camera. However, the periodic intensity distribution of the nonlinear moiré effect is visible at the location of π-phase line (Figure 1) owing to the generated SH destructive interference of opposite ferroelectric domains in the two NPCs.

2.2. Experimental Verification

The schematic of the experimental setup is shown in **Figure 2**. A compact ytterbium-doped diode-pumped ultrafast amplified laser was used to generate 500 fs light pulses with a wavelength of 1030 nm. The pulse repetition rate of the laser was 1 kHz, and the energy of a single pulse was ≈0.1 mJ. The near-parallel FF beam with a spot size of 4 mm^2 was propagated along the z-axis of the periodically poled lithium niobates (PPLNs). The spot size of the FF beam was decreased to 2 mm² by passing it through a reverse beam expander, comprising L_1 and L_2 ($f_1 = 200$ mm; $f_2 = 100$ mm), to increase the energy density. The beam was passed through the NPCs; subsequently, a shortpass filter was used to filter out the near-infrared FF beam, and only the SH of 515 nm was captured by the CCD camera. We built an imaging system comprising a lens (L3) and a CCD camera (Figure 2) with a resolution of ≈13 µm. The resolution of the CCD camera used in our experiment was 2448 × 2048 pixels, and the area of each pixel was 3.45 × 3.45 μm^2. PPLN samples were fabricated via electric field poling and used for the experiment without the loss of generality.[43] The poling direction was along the z-axis of the lithium niobate crystal. In the poling process, the second-order nonlinear coefficient ($\chi^{(2)}$) was permanently reversed via application of a high-voltage pulse to a patterned electrode. Conversely, the linear refractive index of the NPCs remained constant.

Two identical PPLNs with a poling period of 10.92 µm and a thickness of 0.5 mm were used in the experiment to demonstrate the nonlinear moiré effect formed by the nonlinear moiré superlattice. The nonlinear domain structure of PPLN after etching with hydrofluoric acid is shown in **Figure 3**a. The nonlinear structures were not treated with hydrofluoric acid during the experiment process; therefore, they could not be effectively detected using the linear optical method. The nonlinear imaging results of the two PPLNs were shown in Figure 3b,c. Although the orientation of the domain structures was inferred from the imaging results, it was difficult to discern the period parameters owing to the relatively low resolution of the homemade nonlinear imaging system. The phase change in the SH, induced by the oppositely polarized domain area, also inhibited optimal structural imaging. When these two PPLNs were tightly superimposed with angle α, a nonlinear moiré effect was clearly observed (Figure 3d). When the rotation angle (α) between the two PPLNs in the experiment was 6°, the SH period of the nonlinear moiré pattern was 107 µm. The rotation angle between the two PPLNs was calculated to be 5.85° using Equation (5), which is identical to the experimental value. These results indicated that the preparation of a standard nonlinear grating enabled the successful detection of the period of the PPLN using a relatively low-resolution optical system.

2.3. Nondestructive Detection of NPCs with Super Resolution

Subsequently, two PPLNs with different periods were used to demonstrate the application of the nonlinear moiré effect for measurement of the period of the nonlinear structure. We chose one of the PPLNs with a period of 9.27 µm as our standard nonlinear grating. The other nonlinear grating with a period of 8.1 µm was the target detection sample. The thicknesses of the two crystals were 0.5 mm. The individual SH imaging results of these two PPLNs were identical to those obtained in the first experiment and were completely indistinguishable in our imaging system. However, when the two PPLNs were closely superimposed along the same direction (**Figure 4**a, $\alpha = 0°$), the nonlinear moiré pattern was clearly detected along the same direction of two PPLNs in the experiment (Figure 4e). The period of the detected nonlinear moiré pattern corresponding to the relative angle of 0° was 65.55 µm. The periods of the target PPLN were experimentally determined using Equation (5) to be 8.11 or 10.8 µm. The nonlinear moiré patterns corresponding to the relative angles (α) of 0.5°, 4°, and 7.5° are shown in Figure 4b–d, respectively. The theoretically derived angles of the nonlinear moiré patterns were 3° ($\alpha = 0.5°$), 26.5° ($\alpha = 4°$), and 41.5° ($\alpha = 7.5°$), respectively. The experimentally obtained angles of the nonlinear moiré patterns (Figure 4f–h) were 3° ($\alpha = 0.5°$), 25° ($\alpha = 4°$), and 42° ($\alpha = 7.5°$), respectively, which were consistent with the theoretically derived angles. The periods of the nonlinear moiré patterns were 64 µm ($\alpha = 0.5°$), 56.3 µm ($\alpha = 4°$), and 46 µm ($\alpha = 7.5°$). The periods of the target PPLN were calculated, using Equation (5), to be 8.1 or 11.1 µm corresponding to the relative angle of 7.5°. Therefore, the actual period of the target nonlinear PPLN grating was determined to be 8.1 µm.

To further demonstrate the resolution power of the nonlinear moiré effect, we calculated the detection range of the optical system with a resolution of 1 µm ($\Lambda_{moiré} = 1\mu m$) to the SH (**Figure 5**). The structural directions of these two nonlinear gratings were identical, i.e., $\alpha = 0°$ (Figure 5c). The spatial frequency of the nonlinear moiré pattern can be written as $f_{moiré} = 1/\Lambda_{moiré} = 1/\Lambda_1 - 1/\Lambda_2$ using the last term of Equation (4). If the period parameter Λ_1 of the nonlinear grating I is known, then such a nonlinear moiré pattern can be clearly

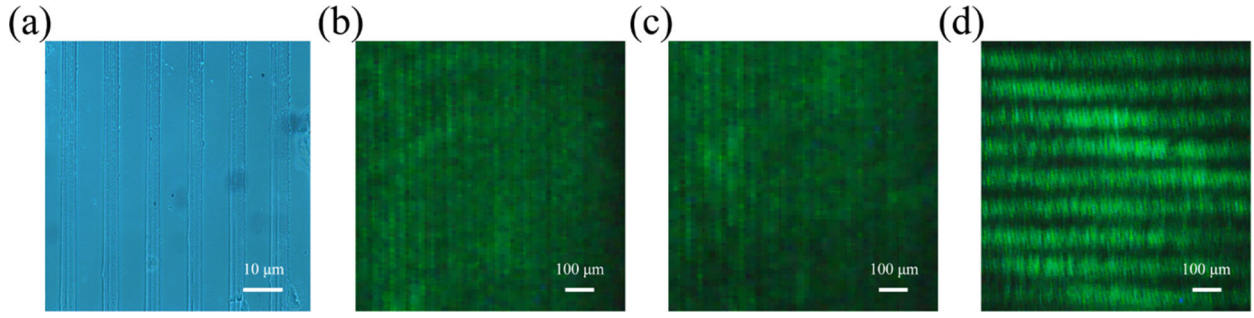

Figure 3. Observation of the nonlinear moiré effect. a) Nonlinear domain structure ($\Lambda = 10.92$ μm) image after etching with hydrofluoric acid. b,c) The nonlinear SH image formed by the two PPLNs and captured using the homemade imaging system with a resolution of ≈13 μm. The structures are indistinct owing to the low resolution of the imaging system. d) The clearly shown nonlinear moiré effect ($\Lambda_{moiré} = 107$ μm with a rotation angle $\alpha = 6°$ of the nonlinear moiré superlattice).

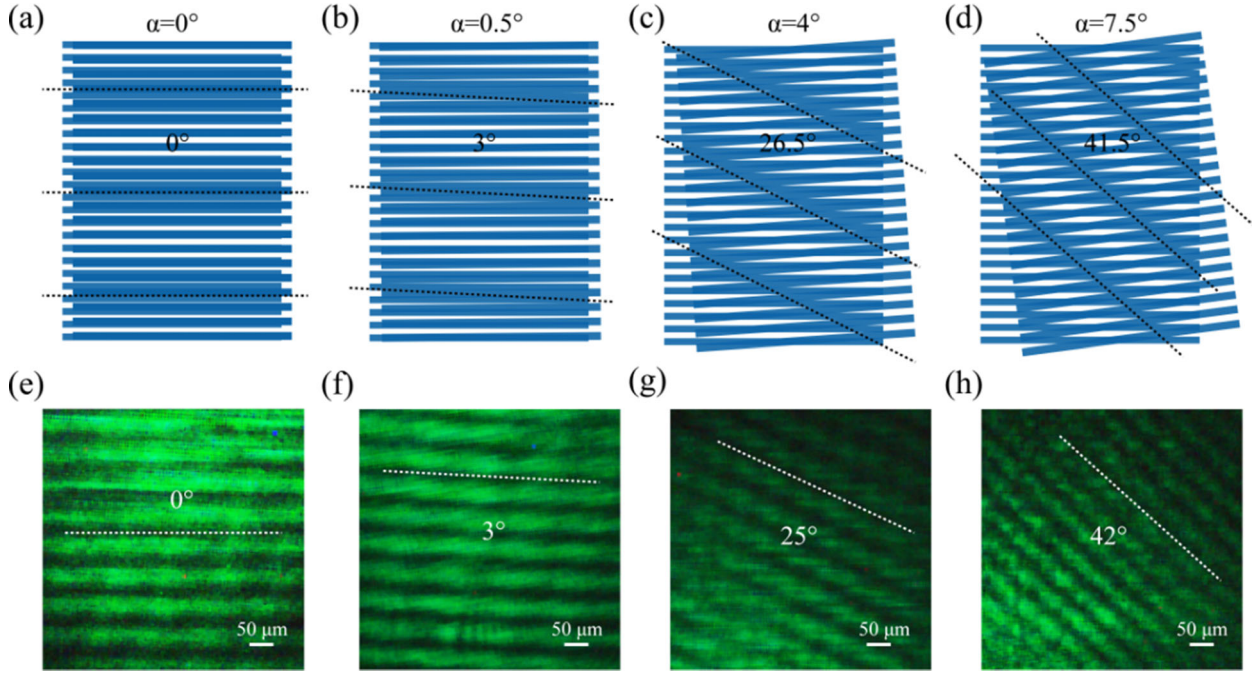

Figure 4. Nonlinear moiré effect changing with varying relative angle (α) when two PPLNs have periods $\Lambda_1 = 9.27$ μm and $\Lambda_2 = 8.1$ μm. The cases of the relative angle are, respectively, a) 0°, b) 0.5°, c) 4°, and d) 7.5°. e–h) Experimental results of the nonlinear moiré effect corresponding to the cases of panels (a)–(d). The periods of the nonlinear moiré patterns are corresponding to 65.55, 64, 56.3, and 46 μm, respectively.

observed by limiting the period parameter (Λ_2) of the nonlinear grating II in the range of $\Lambda_2 > \frac{\Lambda_{moiré} \times \Lambda_1}{\Lambda_{moiré} + \Lambda_1}$ and $\Lambda_2 < \frac{\Lambda_{moiré} \times \Lambda_1}{\Lambda_{moiré} - \Lambda_1}$. The detectable ranges of the nonlinear grating II period were plotted against the changing nonlinear grating I period, and the results for the micro- and nanoscale are presented in Figure 5a and Figure 5b, respectively. The structure parameter of the nonlinear grating II was derived according to the period of the nonlinear moiré effect pattern. Figure 5b shows that the period of the target nonlinear grating was less than 100 nm. Here, the nonlinear moiré effect facilitated detection down to even a few nanometers, provided that several stringent conditions were satisfied. This indicated that the period of the target nonlinear grating should be close to the period of the standard grating. It should be noted that such a nonlinear moiré effect cannot be observed when $\Lambda_2 = \Lambda_1$. However, structural information can still be obtained in this case by changing the twist angle (α). Nevertheless, this period of the target nonlinear grating is significantly lower than the resolution sensitivity of the optical system.

3. Discussion

Light was propagated along the z-axis of the NPCs in the conducted experiments, and the polarization direction of the FF light was along the x-axis of the target nonlinear grating. According to the nonlinear coupled wave equation, the electronic field of the generated SH wave in the standard nonlinear crystal can be written as $\vec{E}(2\omega) = A(2\omega)d_{22}[\sin(2\alpha)\hat{e}_x + \cos(2\alpha)\hat{e}_y]$. Here, α represents the relative rotation angle of the standard nonlinear structure. Therefore, the polarization of the generated SH was approximately entirely along the y-axis of the standard nonlinear

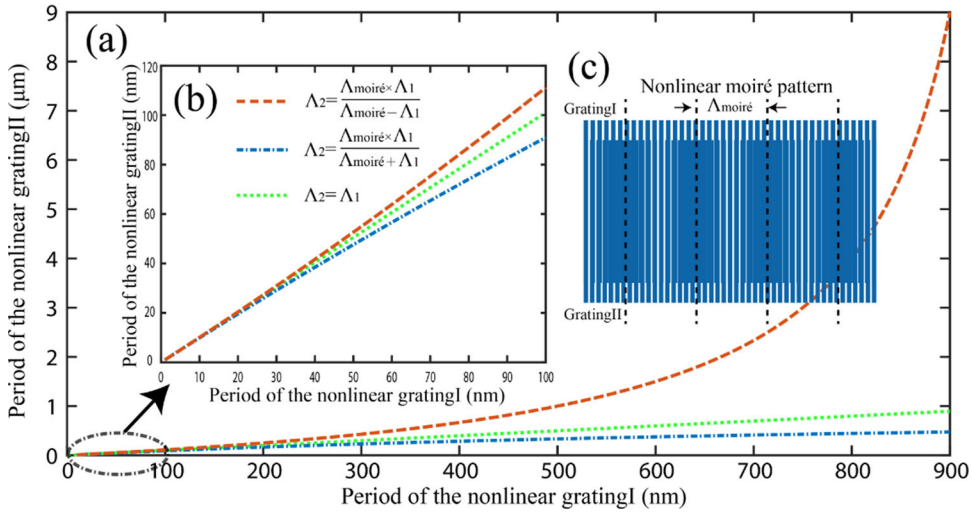

Figure 5. Calculation of the detection range for the nonlinear moiré effect in an optical imaging system with a resolution of 1 μm. a,b) The cases of micro- and nanoscale PPLNs, respectively, in which the nonlinear moiré effect can be observed. c) Formation of the nonlinear moiré effect when two PPLNs are tightly superimposed along the same direction.

grating. This was attributed to the relatively low rotation angle in the experiments. It was inferred that a high relative angle (α) between the two nonlinear gratings influences the contrast of the resulting nonlinear moiré effect. However, this problem can be solved by choosing an appropriate polarization for the incident FF light, thereby ensuring that the nonlinear moiré effect is clearly observed in the experiment. When the thicknesses of two NPCs are different, the contrast of the moiré fringe is lowered owing to the different intensities of the generated SH waves in these two NPCs. However, the generation of the nonlinear moiré effect is not completely influenced. The FF light was incident along the *z*-axis of the NPCs in the present study, which is the phase mismatching process. Therefore, the increase or decrease in the thickness of one NPC did not induce any rapid variation in the SH intensity. This is different from the phase matching process, where the intensity of the SH signal increases with an increase in the nonlinear crystal thickness. The minor difference in contrast of the moiré fringe, owing to the NPC thickness, in the present experiment can be circumvented via a slight change in the incident angle of the FF light. The issue can also be resolved by optimizing the thickness of the standard NPC.

We extended the study of the moiré lattice to the nonlinear optics, which calls it as nonlinear moiré superlattice. Unlike the conventional moiré effect, no real grating was used in our experiment, and the observed nonlinear moiré effect was a consequence of the $\chi^{(2)}$ nonlinear optical process. More importantly, the super-resolution nondestructive detection of the NPCs was achieved using the nonlinear moiré effect. In the future, 1D as well as 2D or arbitrary nonlinear structures may be detected using this method. Our proposition is similar to that in previous studies on super-resolution detection using structured light illumination.[44,45] Therefore, the present study can be treated as the nonlinear version of the structured light illumination approach. A periodically poled NPC can be treated as the standard nonlinear gating, which corresponds to the structured light in a structured light illumination microscope. Arbitrary nonlinear structures can then be detected by tightly superimposing them on the standard nonlinear gating. The spatial resolution in our experiment was superior by a factor of 2 as compared to that of a structured light illumination microscope in linear optics. This was attributed to the low spatial frequency of the SH wave. In principle, if a material facilitates an *N*th-order harmonic generation, the reported nonlinear moiré effect induces an *N*-times increase in the spatial resolution power.

Such a detection method by using nonlinear moiré superlattice can break the resolution of the optical system, which provides a wide-field super-resolution detection manner to NPC. This is the primary difference between the reported detection technique and detection via the nonlinear Talbot effect.[25] In previous studies, such moiré techniques have been applied in some photonic fields, such as optical tweezers[46] and nonlinear solitons.[47] Presumably, the present study is the first to report the application of such moiré techniques in the field of nonlinear imaging. The selection of the optimal twist angle in the 2D nonlinear moiré lattice in future research may result in nonlinear localization.

4. Conclusion

We observed the nonlinear moiré effect originating from the moiré superlattice of two NPCs in the present experiment. The enlarged effect of the nonlinear moiré superlattice facilitated the nondestructive detection of NPCs. The resolution of the demonstrated approach was superior to that of presently used optical systems. Furthermore, we theoretically demonstrated the detection range of the demonstrated method with the prior knowledge about the period of the standard nonlinear grating. The present research conceptually extends the conventional moiré lattice to nonlinear optics, thereby paving the way for new applications based on the sub-micrometer- and nanometer-scale nondestructive detection of NPCs using optical microscopes. Our work also establishes a new field, i.e., NPC moiré superlattices, that will attract substantial research attention in the future. Not limited in the domain of photonics, these nonlinear moiré superlattices

can be extended to other fields where nonlinear effects cannot be avoided, such as polaritons and Bose–Einstein condensates.

Acknowledgements

This work was supported by National Natural Science Foundation of China (NSFC) (Grant Nos. 11734011 and 12004245), National Key Research and Development Program of China (Program Nos. 2018YFA0306301 and 2017YFA0303701), Shanghai Municipal Science and Technology Major Project (Project No. 2019SHZDZX01-ZX06), Shandong Quancheng Scholarship (Grant No. 00242019024), and Startup Fund for Young Faculty at SJTU (Grant No. 21X010500780).

Conflict of Interest

The authors declare no conflict of interest.

Data Availability Statement

The data that support the findings of this study are available from the corresponding author upon reasonable request.

Keywords

nondestructive detection, nonlinear moiré superlattice, nonlinear photonic crystals

Received: December 29, 2020
Revised: May 27, 2021
Published online:

[1] W. F. Lin, J. R. Li, G. Y. Liu, *ACS Nano* **2012**, *6*, 9141.
[2] G. H. Yuan, Q. Wang, X. C. Yuan, *Opt. Lett.* **2012**, *37*, 2715.
[3] H. Miao, A. Panna, A. A. Gomella, E. E. Bennett, S. Znati, L. Chen, H. Wen, *Nat. Phys.* **2016**, *12*, 830.
[4] D. W. Pashley, J. W. Menter, G. A. Bassett, *Nature* **1957**, *179*, 752.
[5] O. Kafri, I. Glatt, *The Physics of Moiré Metrology*, Wiley, New York, NY **1990**.
[6] Y. Cao, V. Fatemi, S. Fang, K. Watanabe, T. Taniguchi, E. Kaxiras, P. Jarillo-Herrero, *Nature* **2018**, *556*, 43.
[7] C. R. Dean, L. Wang, P. Maher, C. Forsythe, F. Ghahari, Y. Gao, J. Katoch, M. Ishigami, P. Moon, M. Koshino, T. Taniguchi, K. Watanabe, K. L. Shepard, J. Hone, P. Kim, *Nature* **2013**, *497*, 598.
[8] P. Wang, Y. Zheng, X. Chen, C. Huang, Y. V. Kartashov, L. Torner, V. V. Konotop, F. Ye, *Nature* **2020**, *577*, 42.
[9] K. Tran, G. Moody, F. Wu, X. Lu, J. Choi, K. Kim, A. Rai, D. A. Sanchez, J. Quan, A. Singh, J. Embley, A. Zepeda, M. Campbell, T. Autry, T. Taniguchi, K. Watanabe, N. Lu, S. K. Banerjee, K. L. Silverman, S. Kim, E. Tutuc, L. Yang, A. H. MacDonald, X. Li, *Nature* **2019**, *567*, 71.
[10] M. Serlin1, C. L. Tschirhart, H. Polshyn, Y. Zhang, J. Zhu, K. Watanabe, T. Taniguchi, L. Balents, A. F. Young, *Science* **2020**, *367*, 900.
[11] V. Berger, *Phys. Rev. Lett.* **1998**, *81*, 4136.
[12] N. G. R. Broderick, G. W. Ross, H. L. Offerhaus, D. J. Richardson, D. C. Hanna, *Phys. Rev. Lett.* **2000**, *84*, 4345.
[13] A. Arie, N. Voloch, *Laser Photonics Rev.* **2010**, *4*, 355.
[14] J. A. Armstrong, N. Bloembergen, J. Ducuing, P. S. Pershan, *Phys. Rev.* **1962**, *127*, 1918.
[15] S. Kuma, Y. Miyamoto, K. Tsutsumi, N. Sasao, S. Uetake, *Opt. Lett.* **2013**, *38*, 2825.
[16] I. Ricciardi, M. De Rosa, A. Rocco, P. Ferraro, A. Vannucci, P. Spano, P. De Natale, *Opt. Lett.* **2009**, *34*, 1348.
[17] R. Das, S. C. Kumar, G. K. Samanta, M. EbrahimZadeh, *Opt. Lett.* **2009**, *34*, 3836.
[18] B. Q. Chen, C. Zhang, C. Y. Hu, R. J. Liu, Z. Y. Li, *Phys. Rev. Lett.* **2015**, *115*, 083902.
[19] M. Baudrier-Raybaut, R. Haidar, P. h. Kupecek, P. h. Lemasson, E. Rosencher, *Nature* **2004**, *432*, 374.
[20] S. M. Saltiel, D. N. Neshev, W. Krolikowski, A. Arie, O. Bang, Y. S. Kivshar, *Opt. Lett.* **2009**, *34*, 848.
[21] A. M. Vyunishev, A. S. Chirkin, *Opt. Lett.* **2015**, *40*, 1314.
[22] Y. Sheng, V. Roppo, Q. Kong, K. Kalinowski, Q. Wang, C. Cojocaru, J. Trull, W. Krolikowski, *Opt. Lett.* **2011**, *36*, 2593.
[23] H. J. Ren, X. W. Deng, Y. L. Zheng, N. An, X. F. Chen, *Phys. Rev. Lett.* **2012**, *108*, 223901.
[24] Y. Q. Qin, C. Zhang, Y. Y. Zhu, X. P. Hu, G. Zhao, *Phys. Rev. Lett.* **2008**, *100*, 063902.
[25] Y. Zhang, J. M. Wen, S. N. Zhu, M. Xiao, *Phys. Rev. Lett.* **2010**, *104*, 183901.
[26] X. H. Hong, B. Yang, C. Zhang, Y. Q. Qin, Y. Y. Zhu, *Phys. Rev. Lett.* **2014**, *113*, 163902.
[27] N. V. Bloch, K. Shemer, A. Shapira, R. Shiloh, I. Juwiler, A. Arie, *Phys. Rev. Lett.* **2012**, *108*, 233902.
[28] T. Ellenbogen, N. Voloch-Bloch, A. Ganany-Padowicz, A. Arie, *Nat. Photonics* **2009**, *3*, 395.
[29] S. Tanzilli, W. Tittel, H. De Riedmatten, H. Zbinden, P. Baldi, M. DeMicheli, D. B. Ostrowsky, N. Gisin, *Eur. Phys. J. D* **2002**, *18*, 155.
[30] H. Jin, P. Xu, X. W. Luo, H. Y. Leng, Y. X. Gong, W. J. Yu, M. L. Zhong, G. Zhao, S. N. Zhu, *Phys. Rev. Lett.* **2013**, *111*, 023603.
[31] J. P. Torres, A. Alexandrescu, S. Carrasco, L. Torner, *Opt. Lett.* **2004**, *29*, 376.
[32] H. Y. Leng, X. Q. Yu, Y. X. Gong, P. Xu, Z. D. Xie, H. Jin, C. Zhang, S. N. Zhu, *Nat. Commun.* **2011**, *2*, 429.
[33] R. Wolf, Y. C. Jia, S. Bonaus, C. S. Werner, S. J. Herr, I. Breunig, K. Buse, H. Zappe, *Optica* **2018**, *5*, 872.
[34] C. Wang, C. Langrock, A. Marandi, M. Jankowski, M. Zhang, B. Desiatov, M. M. Fejer, M. Loncar, *Optica* **2018**, *5*, 1438.
[35] A. Shapira, R. Shiloh, I. Juwiler, A. Arie, *Opt. Lett.* **2012**, *37*, 2136.
[36] V. Y. Shur, A. I. Lobov, A. G. Shur, S. Kurimura, Y. Nomura, K. Terabe, X. Y. Liu, K. Kitamura, *Appl. Phys. Lett.* **2005**, *87*, 022905.
[37] Y. Sheng, A. Best, H. J. Butt, W. Krolikowski, A. Arie, K. Koynov, *Opt. Express* **2010**, *18*, 16539.
[38] R. E. Lu, R. Z. Zhao, X. Feng, B. Yang, X. H. Hong, C. Zhang, Y. Q. Qin, Y. Y. Zhu, *Phys. Rev. Lett.* **2018**, *120*, 067601.
[39] C. Canalias, V. Pasiskevicius, *Nat. Photonics* **2007**, *1*, 459.
[40] S. Katayama, Y. Noguchi, M. Miyayama, *Adv. Mater.* **2007**, *19*, 2552.
[41] P. S. Zelenovskiy, M. D. Fontana, V. Y. Shur, P. Bourson, D. K. Kuznetsov, *Appl. Phys. A* **2010**, *99*, 741.
[42] V. Y. Shur, E. I. Shishkin, E. V. Nikolaeva, M. S. Nebogatikov, D. O. Alikin, P. S. Zelenovskiy, M. F. Sarmanova, M. A. Dolbilov, *Ferroelectrics* **2010**, *398*, 91.
[43] M. Yamada, N. Nada, M. Saitoh, K. Watanabe, *Appl. Phys. Lett.* **1993**, *62*, 435.
[44] M. G. L. Gustafsson, *J. Microsc.* **2000**, *198*, 82.
[45] P. Kner, B. B. Chhun, E. R. Griffis, L. Winoto, M. G. L. Gustafsson, *Nat. Methods* **2009**, *6*, 339.
[46] P. Zhang, D. Hernandez, D. Cannan, Y. Hu, S. Fardad, S. Huang, J. C. Chen, D. N. Christodoulides, Z. Chen, *Biomed. Opt. Express* **2012**, *3*, 1891.
[47] Q. Fu, P. Wang, C. Huang, Y. V. Kartashov, L. Torner, V. V. Konotop, F. Ye, *Nat. Photonics* **2020**, *14*, 663.

